

UCLA

UCLA Previously Published Works

Title

Structural, Computational, and Spectroscopic Investigation of [Pd(κ^3 -1,1'-bis(di-tert-butylphosphino)ferrocenediyl)X]⁺ (X = Cl, Br, I) Compounds

Permalink

<https://escholarship.org/uc/item/6ms3c87q>

Journal

Organometallics, 35(4)

ISSN

0276-7333

Authors

Blass, Brittany L
Sánchez, Raúl Hernández
Decker, Victoria A
[et al.](#)

Publication Date

2016-02-22

DOI

10.1021/acs.organomet.5b00889

Peer reviewed

Structural, computational and spectroscopic
investigation of $[\text{PdX}(\kappa^3\text{-}1,1'\text{-bis(ditert-
butylphosphino)ferrocenediy1})]^+$ (X = Cl, Br or I)
compounds

*Brittany L. Blass,^a Raul Hernández Sánchez,^b Victoria A. Decker,^a Michael J. Robinson,^a
Nicholas A. Piro,^c W. Scott Kassel,^c Paula L. Diaconescu,^d Theodore A. Betley^b and Chip
Nataro*^a*

^aDepartment of Chemistry, Lafayette College, Easton, PA 18042, ^bDepartment of Chemistry and
Chemical Biology, Harvard University, Cambridge, MA 02138, ^cDepartment of Chemistry,
Villanova University, Villanova, PA 19085 and ^dDepartment of Chemistry and Biochemistry,
University of California, Los Angeles, CA 90095

ABSTRACT

INTRODUCTION

1,1'-Bis(diphenylphosphino)ferrocene (dppf) is the bidentate phosphine with a metallocene backbone that has been studied the most, particularly as a ligand in catalytic systems.¹ There are many different types of ligands that are closely related to dppf, but the most

common are ones in which the R groups on the phosphorus atoms are altered (Figure 1). Changing the R groups not only impacts the potential at which oxidation of the iron center occurs,² it can also play a significant role in the reactivity of compounds containing these ligands. In particular, the steric bulk of the *tert*-butyl groups in dtbpf³ has been proposed to be responsible for drastically different behavior that has been observed in several studies of compounds containing this ligand.



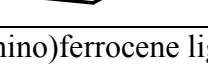
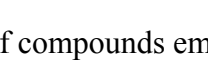
	Ligand	R
	dppf	Ph
	dippf	ⁱ Pr
	dcpf	Cy
	dtbpf	^t Bu

Figure 1. Common bis(phosphino)ferrocene ligands.

The catalytic activity of compounds employing bis(phosphino)ferrocene ligands can be significantly impacted by the steric bulk of dtbpf. The coupling of diphenylphosphine and *o*-CF₃C₆H₄Br was much more efficient with a dippf-Pd(OAc)₂ catalyst precursor than with dtbpf-Pd(OAc)₂.⁴ Of the [Pd(P[∧]P)Cl₂] (P[∧]P = dppf, dippf or dtbpf) catalysts, the dtbpf compound was found to be the least efficient in the cross-coupling of aryl Grignards with bromo-anisoles.⁵ For the allylic amination of a Morita-Baylis-Hillman acetate the catalyst-ligand systems [Pd(C₃H₅)Cl]₂-(P[∧]P) (P[∧]P = dppf, dippf or dtbpf) were similar in terms of product formation, but the dtbpf catalyst gave much higher regioselectivity of the product.⁶ Similarly, the reductive carbonylation of 4-bromoacetanilide using [Pd(dppf)Cl₂] as the catalyst gives predominantly the desired aryl aldehyde product while using [Pd(dtbpf)Cl₂] gives exclusively the arene.⁷ For the [Ru(PPh₃)₃(CO)(H₂)]-(P[∧]P) (P[∧]P = dppf, dippf or dtbpf) catalyzed alkylation of *tert*-butyl ketonitrile with benzyl alcohol, the greater bulk of dtbpf significantly inhibits product formation.⁸

In non-catalytic system, the steric bulk of dtbpf can also play a significant role. Unlike the related 1,1'-bis(phosphine selenide)ferrocene compounds,⁹ oxidation of dtbpfSe₂ results in the formation of an isolable Se-Se bonded dication that has been structurally characterized.^{2d} Reductive elimination of diaryl ethers from [Pd(P[∧]P)(Ar)(OAr')] (P[∧]P = dppf or dtbpf) was found to be significantly faster for the bulkier dtbpf compound.¹⁰ A study of the formation of palladium aryl enolates found that dppf bound as a bidentate ligand to palladium whereas a similar reaction with dtbpf yielded a compound in which only one of the phosphorus atoms of dtbpf was bound to the palladium.¹¹ While two equivalents of B(C₆F₅)₃ will undergo nucleophilic aromatic substitution reactions with dippf to give [Fe(C₅H₄P(ⁱPr)₂C₆F₄BF(C₆F₅)₂)₂], dtbpf only reacts with one equivalent of B(C₆F₅)₃ to give [Fe(C₅H₄P(^tBu)₂C₆F₄BF(C₆F₅)₂)(C₅H₄P(^tBu)₂)]; attempts to drive a reaction with a second equivalent of B(C₆F₅)₃ lead to decomposition.¹²

Of greatest significance to this report are the studies in which dtbpf binds in a κ³-coordination mode to a palladium center (Figure 2). When [Pd(COD)ClCH₃] is reacted with either dppf or dippf the COD is replaced with the bidentate phosphine yielding

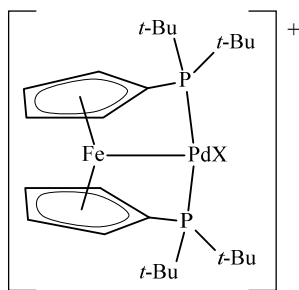


Figure 2. The κ³ coordination mode of dtbpf.

[Pd(P[∧]P)ClCH₃] (P[∧]P = dppf or dippf). However, when a similar reaction is performed with dtbpf the greater steric bulk of the ligand does not allow formation of [Pd(dtbpf)ClCH₃] but instead yields [Pd(κ³-dtbpf)CH₃]Cl.¹³ Similarly, the reaction of Na[BArF] with [Pd(P[∧]P)Cl₂] (P[∧]P = dppf, dippf or dcpf) abstracts a chloride ligand from the palladium and results in the

formation of a dimeric species, $[\text{Pd}_2(\text{P}^\wedge\text{P})_2(\mu\text{-Cl})_2][\text{BArF}]_2$. The bulk of dtbpf prevents this dimerization following chloride abstraction, and thus $[\text{Pd}(\kappa^3\text{-dtbpf})\text{Cl}][\text{BArF}]$ is formed in which the empty coordination site generated by removing a chloride ligand is occupied by a weak, non-covalent interaction between palladium and iron.¹⁴ To further investigate these types of compounds, $[\text{Pd}(\kappa^3\text{-dtbpf})\text{Br}]^+$ was synthesized and characterized by NMR spectroscopy and X-ray crystallography. The nature of the iron-palladium interaction was investigated computationally and compared to the analogous chloride and iodide compounds. In addition, the oxidative electrochemistry and visible spectra of these compounds are compared. Finally, the ^{57}Fe Mössbauer spectra of dtbpf and several compounds containing dtbpf are reported.

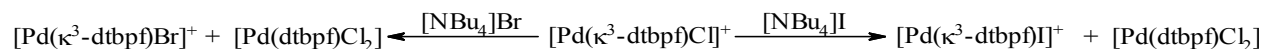
RESULTS AND DISCUSSION

Synthesis and Structural Characterization

Similar to the synthesis of $[\text{Pd}(\kappa^3\text{-dtbpf})\text{Cl}][\text{BArF}]$,¹⁴ the reaction of $[\text{Pd}(\text{dtbpf})\text{Cl}_2]$ with $\text{K}[\text{TFAB}]$ yields $[\text{Pd}(\kappa^3\text{-dtbpf})\text{Cl}][\text{TFAB}]$. To begin to examine the reactivity of $[\text{Pd}(\kappa^3\text{-dtbpf})\text{Cl}]^+$ an NMR tube reaction was performed in which $[\text{PPN}]\text{Cl}$ reacted with $[\text{Pd}(\kappa^3\text{-dtbpf})\text{Cl}]^+$. Unsurprisingly, the ^{31}P NMR spectrum indicated the presence of $[\text{Pd}(\text{dtbpf})\text{Cl}_2]$ (68.7 ppm)¹⁵ and $[\text{PPN}]^+$ (21.7 ppm).¹⁶ Similar reactions were performed adding one equivalent of either $[\text{NBu}_4]\text{Br}$ or $[\text{NBu}_4]\text{I}$ to $[\text{Pd}(\kappa^3\text{-dtbpf})\text{Cl}]^+$. In these reactions the expected asymmetric dihalides, $[\text{Pd}(\text{dtbpf})\text{ClX}]$ ($X = \text{Br}$ or I), did not form. This was somewhat surprising as the compound formulated $[\text{Pd}(\text{dtbpf})\text{Br}_2]$ has been reported and is commercially available.¹⁷ The NMR tube reaction of $[\text{Pd}(\kappa^3\text{-dtbpf})\text{Cl}]^+$ with $[\text{NBu}_4]\text{Br}$ yielded an approximately 3:5 mixture of $[\text{Pd}(\text{dtbpf})\text{Cl}_2]$ and $[\text{Pd}(\kappa^3\text{-dtbpf})\text{Br}][\text{TFAB}]$ while the reaction with $[\text{NBu}_4]\text{I}$ gave $[\text{Pd}(\text{dtbpf})\text{Cl}_2]$ and $[\text{Pd}(\kappa^3\text{-dtbpf})\text{I}]^+$ in an approximately 1:10 ratio (Scheme 1). Formation of $[\text{Pd}(\text{dtbpf})\text{ClX}]$ (X

= Br or I) is apparently unfavorable due to steric constraints. However, ligand substitution of the chloride ligand in $[\text{Pd}(\kappa^3\text{-dtbpf})\text{Cl}]^+$ occurs with the stronger field halides. The free chloride that is generated can then react with $[\text{Pd}(\kappa^3\text{-dtbpf})\text{Cl}]^+$ to yield $[\text{Pd}(\text{dtbpf})\text{Cl}_2]$. Based on the ratio of the products, it would appear that the iodide reacts significantly faster than the bromide.

Scheme 1. Reactions of $[\text{Pd}(\kappa^3\text{-dtbpf})\text{Cl}]^+$ with $[\text{NBu}_4]\text{X}$ ($\text{X} = \text{Br}^-$ or I^-).



Although $[\text{Pd}(\text{dtbpf})\text{Br}][\text{TFAB}]$ was isolated by scaling up the aforementioned reaction, it is not an efficient synthesis as approximately half of the starting material is converted to $[\text{Pd}(\text{dtbpf})\text{Cl}_2]$. Based on the synthesis of $[\text{Pd}(\text{dtbpf})\text{I}][\text{I}]$,¹⁸ $[\text{Pd}(\text{dtbpf})\text{Cl}_2]$ reacted with excess NaBr to yield $[\text{Pd}(\text{dtbpf})\text{Br}][\text{Br}]$. In addition, $[\text{Pd}(\text{dtbpf})\text{Cl}]^+$ was found to react with either NaBr or NaI to give the corresponding $[\text{Pd}(\text{dtbpf})\text{X}]^+$ ($\text{X} = \text{Br}$ or I). The ^{31}P NMR signal for $[\text{Pd}(\text{dtbpf})\text{Br}]^+$ is at 11.5 ppm, similar to that observed for the corresponding chloride and iodide cations.

The structure of $[\text{Pd}(\text{dtbpf})\text{Br}][\text{TFAB}]$ was determined (Figure 3) over a range of temperatures. Similar to $[\text{Pd}(\text{dtbpf})\text{Cl}][\text{SbCl}_6]$,¹⁴ the structure of $[\text{Pd}(\text{dtbpf})\text{Br}][\text{TFAB}]$ undergoes a reversible isomerization in the solid state. At room

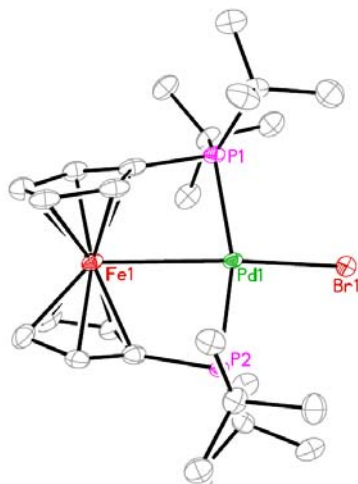


Figure 3. Perspective view of [Pd(dtbpf)Br][TFAB] with 30% ellipsoids at 100(2) K. Hydrogen atoms and [TFAB]⁻ are omitted for clarity.

temperature, the only form present is the κ^3 -dtbpf structure shown in Figure 3. This isomer displays an Fe–Pd distance similar to that found in the chloride¹⁴ and iodide¹⁸ analogs. A second isomer in which the dtbpf is coordinated in a κ^2 coordination mode is observed at lower temperatures (see Supporting Information). This second isomer was previously described as being three-coordinate,¹⁴ however further analysis suggests that this description is not appropriate. The low temperature isomers of [Pd(dtbpf)X]⁺ (X = Cl or Br) display two significantly different P–Pd–X angles of approximately 105° and 150°. In addition, both structures display several short (approximately 2.7 Å) contacts between the palladium atom and the idealized positions for the hydrogen atoms of the *tert*-butyl groups. These observations suggest that the low temperature isomer is also four-coordinate with the fourth coordination site being occupied by an agostic interaction with the *tert*-butyl groups. However, even at temperatures approaching the freezing point of the CDCl₃ solvent there were no indications of this interaction in the ¹H NMR spectrum of either compound.

The closely related structure of [Pd(dtbpf)I][I] has been reported at 150 K.¹⁸ The structure was determined at several temperatures (Supporting Information) and while the space group changed from P_{bca} to $P2_1/c$, there was no evidence of isomerization. In comparing the structures of [Pd(dtbpf)X]⁺ (X = Cl, Br or I) (Table 1), the Fe–Pd distances are all significantly longer than 2.71 Å, the sum of the covalent radii.¹⁹ The C₅ rings are tipped from being parallel by approximately 20° and the angle increases as the size of the halide increases. As seen in related compounds,^{14, 18} this tip causes a significant difference in the chemical shifts of the H_α and H_β protons of the C₅ rings in the ¹H NMR spectrum. The percent buried volume (%V_{bur}) is a measurement of the space a ligand occupies around a metal center.^{3a} The calculated²⁰ %V_{bur} values for the dtbpf ligand in this series of compounds decreases slightly as the size of the coordinated halide increases.

Table 1. Selected distances (Å), angles (°), and structural parameters for [Pd(dtbpf)Cl][SbCl₆], [Pd(dtbpf)Br][TFAB] and [Pd(dtbpf)I][I] at 100(2) K.

	[Pd(dtbpf)Cl][SbCl ₆] ¹⁴	[Pd(dtbpf)Br][TFAB]	[Pd(dtbpf)I][I]
Fe–Pd	2.977(7)	2.9395(18)	2.9390 ^a
Pd–P(1)	2.310(9)	2.3012(15)	2.2876 ^a
Pd–P(2)	2.280(9)	2.2904(15)	2.2892 ^a
Pd–X	2.336(7)	2.4494(14)	2.5970 ^a
P–Pd–P	162.5(4)	163.04(5)	161.88 ^a
P–Pd–Fe (avg.)	81.4	81.52	80.98 ^a
P–Pd–X (avg.)	98.6	98.42	99.08 ^a
%V _{bur}	73.0	72.1	71.7 ^a
ϕ	17.5(10)	19.27(14)	20.76 ^a
τ^c	41.4(16)	41.7(2)	40.6 ^a
δ_p^d	0.09(4)	0.118(5)	0.141 ^a
	0.06(4)	0.125(5)	0.116 ^a
Cent. –Fe–Cent. ^e	162.5(6)	160.72(10)	161.28 ^a

^aAverage of two crystallographically independent molecules in the unit cell. ^bThe tilt angle of the two C₅ rings. ^cThe torsion angle formed between C_a–Cent._a–Cent._b–C_b, with C being the carbon atom bonded to phosphorus and Cent. the centroid of the C₅ ring. ^dThe distance between the P atoms and the C₅ plane; a positive value means the P atom is closer to Fe. ^eThe angle formed between the centroid of each C₅ ring and the Fe center.

Two other techniques were employed to further examine the Fe–Pd interaction in these compounds. The visible spectrum of these compounds displays a single absorbance that can be attributed to Fe d-d transitions (Table 2).²¹ The λ_{max} values shift to higher wavelengths as the donor ability of the halide increases. This is opposite of the trend observed in

Table 2. Visible absorbance data for approximately 0.2 mM solutions in CH₂Cl₂.

Compound	λ_{max} (nm)	ϵ (M ⁻¹ cm ⁻¹)
dtbpf	458	270
[Pd(dtbpf)Cl][TFAB]	450	3600
[Pd(dtbpf)Br][Br]	455	5200
[Pd(dtbpf)I][I]	478	5500

[Pd(dtbpf)PR₃]⁺² (PR₃ = PBu₃, PPh₂Me or PPh₃),²² [Pd((C₅H₅ER)₂Fe)PPh₃]⁺² (E = S or Se; R = Me or Ph),²³ and [Ru(PR₃)₂((C₅H₄NH)₂Fe)] (PR₃ = PMe₂Ph or PPh₃),²⁴ in which the weaker σ -donor ligands trans to iron display the higher wavelength absorbance. Similar to [Pd(dtbpf)CH₃]⁺,²⁵ there were no absorbance indicative of an Fe–Pd interaction at higher wavelengths. Such bands are noted in [Ru(PR₃)₂((C₅H₄NH)₂Fe)] (PR₃ = PMe₂Ph or PPh₃),²⁴ which have been calculated to have stronger Fe–Ru interactions than the Fe–Pd interactions in these systems.

Mössbauer Spectroscopy

To further investigate the nature of the Fe–Pd interaction, zero-field ⁵⁷Fe Mössbauer spectra were collected on dtbpf, [Pd(dtbpf)Cl₂], and [Pd(dtbpf)X]⁺ (X = Cl or Br) (Figure 4 and S8-10). At 90 K, dtbpf has an isomer shift (δ) and quadrupole splitting ($|\Delta E_Q|$) of 0.54 and 2.35 mm/s, respectively (Figure 4f and S8). This is almost identical to ferrocene²⁶ and in line with other ferrocene compounds.^{26, 27} Complexation of PdCl₂ shifts δ and $|\Delta E_Q|$ to 0.49 and 2.27 mm/s, respectively (Figure 4f and S9). The geometry at

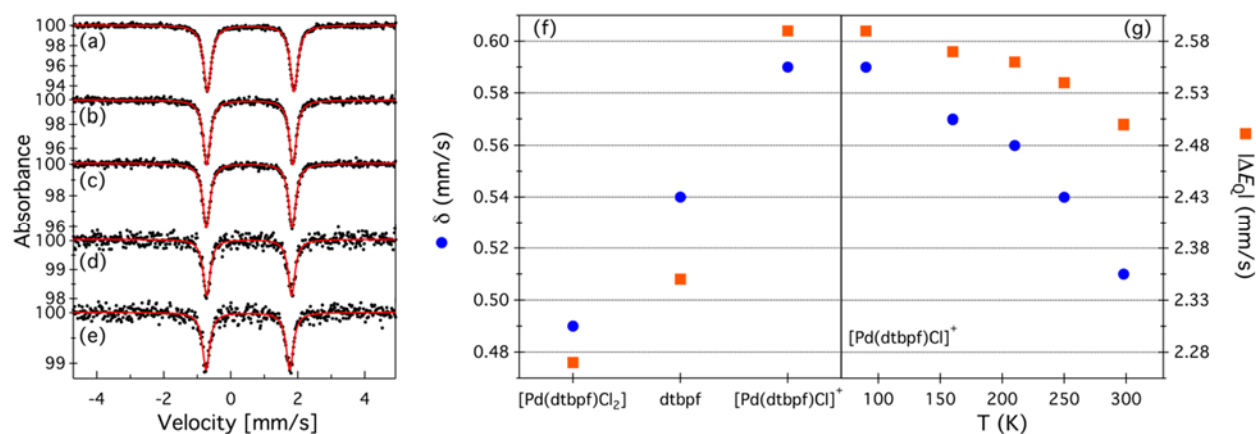


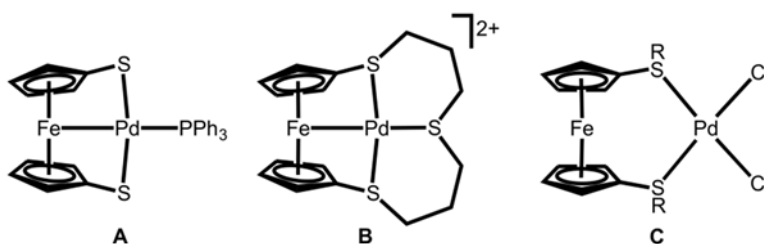
Figure 4. Variable-temperature zero-field ^{57}Fe Mössbauer spectra for $[\text{Pd}(\text{dtbpf})\text{Cl}][\text{SbCl}_6]$: (a) 90, (b) 160, (c) 210, (d) 250, and (e) 298 K. (f) Isomer shift (δ) and quadrupole splitting ($|\Delta E_Q|$) parameters for dtbpf, $[\text{Pd}(\text{dtbpf})\text{Cl}_2]$, and $[\text{Pd}(\text{dtbpf})\text{Cl}][\text{SbCl}_6]$ at 90 K. (g) δ and $|\Delta E_Q|$ parameters extracted from (a-e).

the coordinated metal has been observed to play an important role on the resulting Mössbauer parameters; square planar species tend to have smaller δ and $|\Delta E_Q|$, followed by octahedral species with slightly perturbed values, and ultimately tetrahedral complexes with larger parameters relative to ferrocene.²⁸ These findings correlate directly with the Fe–Cent. distance to the center of each Cp ring: the shortest values are found for square planar and the longest for tetrahedral complexes.²⁸ While the structure of dtbpf has not been reported, the Fe–Cent. distance in the closely related (S,S)-1,1',3-tris(di-*t*-butylphosphino)-2'-(1-N,N-dimethylaminoethyl)-ferrocene (1.670 Å)²⁹ is longer than in $[\text{Pd}(\text{dtbpf})\text{Cl}_2]$ (1.634 Å)^{17a} and thus one expects a lower isomer shift for the Pd adduct due to greater electron density withdrawal from the iron center.

As discussed previously, removal of a chloride from $[\text{Pd}(\text{dtbpf})\text{Cl}_2]$ produces the cationic $[\text{Pd}(\text{dtbpf})\text{Cl}]^+$ complex.¹⁴ In $[\text{Pd}(\text{dtbpf})\text{Cl}]^+$, the extent of the Fe–Pd interaction varies with temperature as determined by the change in the Fe–Pd distance at 100 and 296 K (Table 3). There are very few examples of compounds containing κ^3 -ferrocenyl moieties as ligands that have reported both structural and Mössbauer data. In fact, from an in-depth survey of the

literature, only two examples were found where Mössbauer spectra are reported at low (77 K) and high (~298 K) temperatures, namely compounds **A** and **B**. The variable-temperature spectral and structural behavior of the latter two and of the square planar κ^2 -ferrocenyl compound **C** and [Pd(dtbpf)Cl₂] are used as references for those reported here, displaying a small percentage of molecules isomerizing between long and short Fe–Pd distances (Table 3). To probe the temperature-dependent isomerization in

Table 3. Crystallographic and ⁵⁷Fe Mössbauer parameters for species containing short and long Fe–Pd distances.



Compound	$d_{\text{Fe-Pd}}$ (Å) / T (K)	T range (K)	$\Delta\delta$ (mm/s)	$\Delta \Delta E_Q $ (mm/s)
A	2.878(1) / 298 ^a	77 – RT ^{b, c}	0.05	0.04
B	2.827(2) / 275 ^d	77 – RT ^{b, c}	0.08	0.03
C	3.810(2) / 275 ^e	77 – RT ^{b, f}	0.05	0.05
[Pd(dtbpf)Cl ₂]	4.4026(11) ^g	90 – 298	0.09	0.05
[Pd(dtbpf)Cl] ⁺	2.9389(6) / 296 ^h 4.41(1) / 100 ^{h, i}	90 – 298	0.08	0.09
[Pd(dtbpf)Br] ⁺	2.9285(6) / 295 4.292(12) / 100 ⁱ	90 – 298	0.07	0.04

^aReference 30. ^bRT stands for room temperature. ^cReference 31. ^dReference 32. ^eR = ⁱBu Reference 33. ^fR = Me Reference 23. ^gReference 17a. ^hReference 14. ⁱDistance observed in the minor component (<10%).

[Pd(dtbpf)Cl]⁺ and [Pd(dtbpf)Br]⁺, Mössbauer spectra were collected at 90, 160, 210, 250, and 298 K (Figure 4a-e and Figure S10). The resulting δ and $|\Delta E_Q|$ obtained from fitting the data are shown in Figure 4g (for X = Br, see Figure S11). The decrease in δ as the temperature rises can be explained by the second order Doppler effect³⁴ and, hypothetically, by full conversion to the

shorter Fe–Pd interaction at room temperature. In related complexes with a proposed Fe–Pd interaction, $\Delta\delta$ ranges from about 0.05 to 0.08 mm/s at low (77 K) and high (298 K) temperature (Table 3). The $\Delta\delta_{90-298\text{ K}}$ in $[\text{Pd}(\text{dtbpf})\text{Cl}]^+$ and $[\text{Pd}(\text{dtbpf})\text{Br}]^+$ is 0.08 and 0.07 mm/s, respectively; thus the Fe–Pd interaction formed at high temperature seems to have little effect on the value of δ .

In contrast to δ , the quadrupole splitting ($|\Delta E_Q|$) has been proposed to be more sensitive when equatorial interactions are proposed in ferrocene compounds.³⁰ It is well known that $|\Delta E_Q|$ has an almost negligible variation with temperature and thus any interaction with the iron atom in ferrocene compounds can be diagnosed via this parameter.³¹ In Table 3, two examples are given with a short (**A**, **B**) and two with a long Fe–Pd distance (**C**, $[\text{Pd}(\text{dtbpf})\text{Cl}_2]$). Regardless of the presence of an Fe–Pd interaction, the temperature variation between 77 and 298 K of $|\Delta E_Q|$ on these four examples is approximately 0.04 mm/s on average. Thus, the observed $\Delta|\Delta E_Q|_{90-298\text{ K}}$ of 0.09 mm/s in $[\text{Pd}(\text{dtbpf})\text{Cl}]^+$ is proposed to be the result of the sum of two effects: (1) the standard temperature dependence observed in related compounds (Table 3: **A–C** and $[\text{Pd}(\text{dtbpf})\text{Cl}_2]$), and (2) the formation of a weak Fe–Pd interaction. Further support for the Fe–Pd interaction in $[\text{Pd}(\text{dtbpf})\text{Cl}]^+$ is gained when comparing the Mössbauer data reported for $[\text{Pd}(\text{dppf})(\text{PPh}_3)][\text{BF}_4]_2$ ($d_{\text{Fe-Pd}} = 2.877(2)$ Å) and $[\text{Pd}(\text{dppf})(4\text{-picoline})_2][\text{BF}_4]_2$ (^1H NMR spectroscopic data suggest a long Fe–Pd distance).²² The former compound, with a short Fe–Pd distance, displays Mössbauer parameters of $[\delta, |\Delta E_Q|$ (mm/s): 0.51(1), 2.24(1)], whereas the latter compound has $[\delta, |\Delta E_Q|$ (mm/s): 0.57(1), 2.61(1)].²⁴ In contrast, the Mössbauer data of $[\text{Pd}(\text{dtbpf})\text{Br}]^+$ indicates $\Delta\delta_{90-298\text{ K}}$ and $\Delta|\Delta E_Q|_{90-298\text{ K}}$ that suggests that there is a negligible change in the extent of the Fe–Pd interaction between low (90 K) and high (298 K) temperature (Figure S11).

Electrochemistry

The electrochemistry of [Pd(dtbpf)Br][Br] was examined using cyclic voltammetry. Similar to the analogous chloride, the oxidative electrochemistry displays a single, chemically reversible wave (Table 4). This wave is due to the oxidation of the iron center. The trend in the potentials follows what is predicted by the computational analysis (vide infra); as the strength of

Table 4. Electrochemical data for [Pd(dtbpf)X]⁺ (X = Cl, Br or I) compounds.^a

	E°	ΔE	E_p	E_p
[Pd(dtbpf)Cl] ⁺	0.94 ^b	0.07 ^b	-1.01 ^c	-1.61 ^c
[Pd(dtbpf)Br] ⁺	0.92	0.08	-0.90	-1.56
[Pd(dtbpf)I] ⁺	0.88 ^{b, d}	0.11 ^b	-0.58 ^b	-0.85 ^b

^a Potentials are in V vs. FcH^{0/+}. ^b Reference 14. ^c In CH₂Cl₂ with [NBu₄][TFAB] as the supporting electrolyte. ^d Irreversible oxidative waves due to the iodide counter ion are also observed.

the Fe-Pd interaction increases, the potential at which the oxidation of iron occurs becomes more positive, although it is important to note the small changes between the three compounds. The reductive electrochemistry of [Pd(dtbpf)Br]⁺ displays two irreversible waves attributed to reduction of the palladium. Previously, the reductive electrochemistry of [Pd(dtbpf)Cl]⁺ was reported to display one irreversible wave, while [Pd(dtbpf)I]⁺ displayed two irreversible waves.¹⁴ The reductive electrochemistry of [Pd(dtbpf)Cl]⁺ was examined using [NBu₄][TFAB] as the supporting electrolyte and it was found to display two irreversible waves (Figure 5). The trend in the reduction potentials follows what was observed with oxidation; [Pd(dtbpf)Cl]⁺ is the most difficult to reduce due to greater electron donation from the iron.

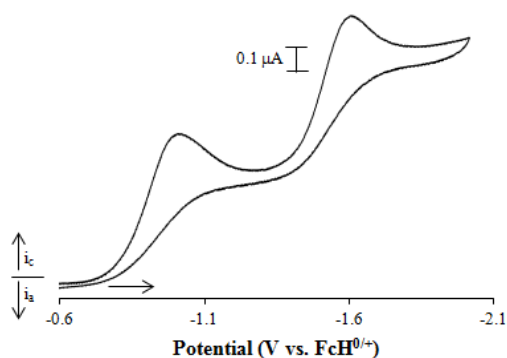


Figure 5. Cyclic voltammogram for the reduction of 1.0 mM [Pd(dtbpf)Cl][TFAB] in CH₂Cl₂/0.05 M [NBu₄][TFAB] at a glassy carbon electrode and a scan rate of 100 mV/s.

Computational Studies

Compounds [Pd(dtbpf)Cl]⁺ and [Pd(dtbpf)I]⁺ were previously examined by computational methods, however, because a different version of the software was available, calculations were repeated for these compounds as well (Table 5). Geometry optimizations for [Pd(dtbpf)X]⁺ (X = Cl, Br, I) were performed for the present study employing ADF2013.01⁴⁷, using the PW91 functional and no frozen electron cores.⁴⁸ The optimized Fe→Pd distance (2.99 Å) for [Pd(dtbpf)Br]⁺ is close to that obtained experimentally (2.94 Å) as are other structural parameters (Table S1). The calculated Mayer bond order⁴⁹ for the [Pd(dtbpf)Br]⁺ is 0.32 and is similar to the values obtained for the chloride and iodide analogues (Table 5). These values are smaller than those reported for metal-metal single bonds in [Ru(CO)₄]₈ (0.70) and Ru₃(CO)₁₂ (0.62),⁵⁰ but they are similar to those reported for [((C₅H₄NH)₂Fe)Ru(PR₃)₂] (PR₃ = PPh₃, 0.28, and PMe₂Ph, 0.26).²⁴

Table 5. Computational parameters for [Pd(dtbpf)X]⁺ (X = Cl or I).

	[Pd(dtbpf)Cl] ⁺	[Pd(dtbpf)Br] ⁺	[Pd(dtbpf)I] ⁺
Fe-Pd (Å)	2.98	2.99	2.99
Mayer Bond Order	0.34	0.32	0.30
Mulliken Charges			
Fe	-0.12	-0.12	-0.11
Pd	-0.46	-0.43	-0.67

Hirshfeld Charges			
Fe	0.05	0.05	0.05
Pd	0.34	0.32	0.30
Wiberg bond index	0.13	0.12	0.11
NLMO Bond Order	0.13	0.14	0.14
Natural Charge			
Fe	0.20	0.20	0.20
Pd	0.33	0.29	0.21
Bader Charge			
Fe	0.71	0.72	0.71
Pd	0.20	0.15	0.04
ρ at Fe-Pd BCP*	0.02	0.02	0.02
Laplacian ($\nabla^2\rho$) at Fe-Pd BCP	0.03	0.03	0.03

* BCP is a bond critical point identified by Bader analysis.

Two significant bonding interactions were found between iron and palladium in $[\text{Pd}(\text{dtbpf})\text{Br}]^+$ (HOMO-4 and HOMO-5) (Figure 6). These orbitals have a relatively large contribution from the metal atomic orbitals (see the supporting information for details): HOMO-4 (39% Pd and 29% Fe) and HOMO-5 (14% Pd and 12% Fe).

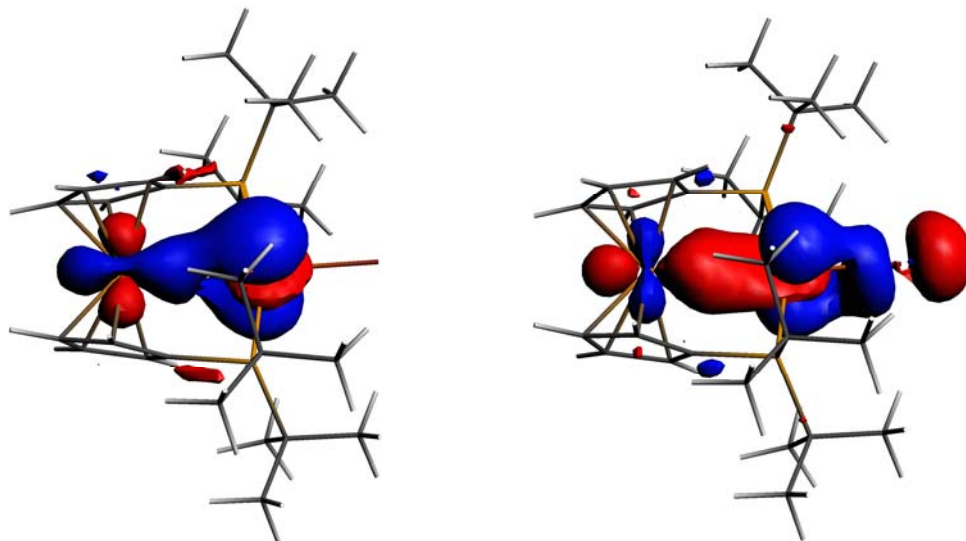


Figure 6. Frontier molecular orbitals for $[\text{Pd}(\text{dtbpf})\text{Br}]^+$: HOMO-4 (left) and HOMO-5 (right); isosurface value = 0.03.

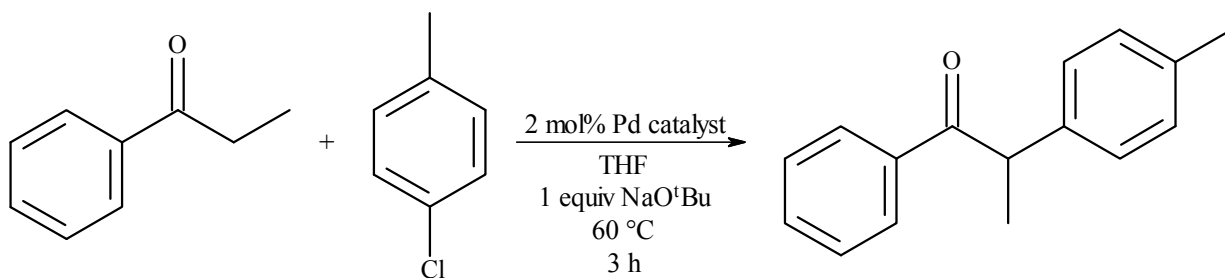
In order to understand further the Fe→Pd interaction, natural bond orbital analysis was carried out using NBO 6.0,⁵¹ and the natural localized molecular orbitals (NLMOs) were generated. For [Pd(dtbpf)Br]⁺, a σ bond is apparent in NLMO 87, which is centered on iron, similarly to what was found for [Pd(dtbpf)Cl]⁺ (NLMO 79) and for [Pd(dtbpf)I]⁺ (NLMO 96) (see the supporting information for details).

Topological analysis of the electron density was performed via Bader's atoms in molecule (AIM) theory.⁵² AIM identifies bonds by calculating (3, -1) critical points, and it differentiates between covalent bonds and weak interactions, such as hydrogen bonds, van der Waals, and donor-acceptor interactions, by the value of the Laplacian ($\nabla^2\rho$). If $\nabla^2\rho < 0$, the interaction is considered covalent. If $\nabla^2\rho > 0$, the interaction is a weak interaction. AIM has been used to calculate bond critical points between two metal centers⁵³ and in ferrocene complexes.⁵⁴ All three [Pd(dtbpf)X]⁺ species show Fe-Pd bond critical points (Table 5) consistent with a weak, non-covalent interaction (see the supporting information for details).

Catalytic Studies

To further examine the effect of changing the halide, the catalytic activity of the [Pd(dtbpf)X]⁺ (X = Cl, Br or I) and [Pd(dtbpf)Cl₂] was examined in the α -arylation of propiophenone with 4-chlorotoluene (Scheme 2). Previous reports have examined

Scheme 2. Palladium catalyzed α -arylation of propiophenone with 4-chlorotoluene.



this same reaction using $[\text{Pd}(\text{dtbpf})\text{Cl}_2]$, $[\text{Pd}(\text{dtbpf})\text{Br}_2]$ and $[\text{Pd}(\text{dtbpf})\text{I}_2]$ as the catalysts precursors.¹⁷ Although those studies report the use of $[\text{Pd}(\text{dtbpf})\text{Br}_2]$ and $[\text{Pd}(\text{dtbpf})\text{I}_2]$, it is likely that the compounds that were actually employed were $[\text{Pd}(\text{dtbpf})\text{Br}]^+$ and $[\text{Pd}(\text{dtbpf})\text{I}]^+$. At the writing of this manuscript, the only known reports of $[\text{Pd}(\text{dtbpf})\text{Br}_2]$ do not include synthetic details or any characterization data.¹⁷ While those same reports suggest the use of $[\text{Pd}(\text{dtbpf})\text{I}_2]$, there is evidence that the compound used was actually $[\text{Pd}(\text{dtbpf})\text{I}][\text{I}]$.³⁷ Using similar conditions to the previous report (Table 5)

Table 6. Catalytic activity of palladium compounds for the α -arylation of propiophenone with 4-chlorotoluene.

Palladium Catalyst	TON^a
None	0
$[\text{Pd}(\text{dtbpf})\text{Cl}_2]$	221(8)
$[\text{Pd}(\text{dtbpf})\text{Cl}]^+$	81(2)
$[\text{Pd}(\text{dtbpf})\text{Br}]^+$	62(3)
$[\text{Pd}(\text{dtbpf})\text{I}]^+$	2(1)

^a Turnover number is the average of three experiments reported with the average deviation from the mean.

As the catalytic study was performed in THF, the $^{31}\text{P}\{^1\text{H}\}$ NMR spectra of the palladium compounds were obtained in THF and found to be similar to those obtained in CH_2Cl_2 (differing only slightly in the chemical shifts) with the exception of $[\text{Pd}(\text{dtbpf})\text{Br}]^+$. A sample of $[\text{Pd}(\text{dtbpf})\text{Br}]^+$ dissolved in CH_2Cl_2 gave a single peak in the $^{31}\text{P}\{^1\text{H}\}$ spectrum. When solvent was removed in vacuo and the sample was dissolved in THF, five peaks were observed. The spectra were then recorded from 35 to $-65\text{ }^\circ\text{C}$ in $10\text{ }^\circ\text{C}$ intervals. The spectra displayed five peaks from 35 to $-5\text{ }^\circ\text{C}$ and six peaks at lower temperatures (Table 6). While none of these species were isolated, it is possible to propose a reasonable formula based on the available data. The peak at 12.4 ppm is $[\text{Pd}(\text{dtbpf})\text{Br}]^+$ and this remains the predominant species in solution at all temperatures. The four signals in the 60-70 ppm range are likely due to four coordinate species,

in which there is no interaction between the iron and palladium centers. An approximately 50 ppm downfield shift is also observed in comparing $[\text{Pd}(\text{dtbpf})\text{Cl}]^+$ to $[\text{Pd}(\text{dtbpf})\text{Cl}_2]$.¹⁴ The two doublets are likely due to an asymmetric compound, which is proposed to be $[\text{Pd}(\text{dtbpf})\text{Br}(\text{thf})]^+$. The remaining two peaks are likely due to symmetric species, which are proposed to be $[\text{Pd}(\text{dtbpf})\text{Br}_2]$ and $[\text{Pd}(\text{dtbpf})(\text{thf})_2]^{+2}$. Presumably, the larger signal at 65.3 ppm is due to $[\text{Pd}(\text{dtbpf})\text{Br}_2]$. The species that appears at -15 °C is shifted downfield by approximately 20 ppm from the proposed signal for $[\text{Pd}(\text{dtbpf})\text{Br}_2]$. A similar difference in chemical shifts is noted in comparing $[\text{Pd}(\text{dppf})\text{Cl}_2]$ and $[\text{Pd}_2(\text{dppf})_2(\mu\text{-Cl})_2]^{+2}$,¹⁴ suggesting that the peak at 83.0 ppm could be due to the formation of $[\text{Pd}_2(\text{dtbpf})_2(\mu\text{-Br})_2]^{+2}$. When THF was removed in vacuo from this sample and the solid was dissolved in CH_2Cl_2 , the $^{31}\text{P}\{^1\text{H}\}$ NMR spectrum displayed a single peak for $[\text{Pd}(\text{dtbpf})\text{Br}]^+$. Similar behavior is not observed for $[\text{Pd}(\text{dtbpf})\text{Cl}]^+$, likely due to the fact that the counter anion is not chloride; as reported above, the addition of chloride to $[\text{Pd}(\text{dtbpf})\text{Cl}]^+$ cleanly results in the formation of $[\text{Pd}(\text{dtbpf})\text{Cl}_2]$. For $[\text{Pd}(\text{dtbpf})\text{I}]^+$, the larger iodide and/or the stronger donor ability of iodide may prevent the formation of species such as $[\text{Pd}(\text{dtbpf})\text{I}_2]$. This could be additional evidence for why $[\text{Pd}(\text{dtbpf})\text{I}]^+$ is a significantly less effective catalyst for this α -arylation reaction (Table 5).

Table 7. Variable temperature $^{31}\text{P}\{^1\text{H}\}$ NMR spectroscopic data for $[\text{Pd}(\text{dtbpf})\text{Br}]\text{Br}$ in THF.

Peak (ppm)	Mult.	$^2J_{\text{P-F}}$ (Hz)	Relative Integration											
			35 °C	25 °C	15 °C	5 °C	-5 °C	-15 °C	-25 °C	-35 °C	-45 °C	-55 °C	-65 °C	
12.4	s		1.00	1.00	1.00	1.00	1.00	1.00	1.00	1.00	1.00	1.00	1.00	1.00
62.5	d	35	0.12	0.13	0.12	0.12	0.13	0.14	0.11	0.12	0.14	0.12	0.13	
63.9	s		0.04	0.02	0.03	0.03	0.03	0.04	0.02	0.03	0.04	0.02	0.06	
65.3	s		0.42	0.47	0.52	0.54	0.57	0.58	0.59	0.60	0.64	0.64	0.65	
66.7	d	35	0.13	0.11	0.12	0.10	0.15	0.13	0.11	0.16	0.16	0.14	0.16	
83.0	s							0.07	0.10	0.14	0.11	0.13	0.11	

EXPERIMENTAL SECTION

General Considerations. All reagents were used as received unless otherwise indicated.

$[\text{PdCl}_2(\text{MeCN})_2]$, sodium tetrafluoroborate, isopropylmagnesium chloride (2.0 M in THF), 1,3-

bis(trifluoromethyl)-5-bromobenzene, tetrabutylammonium bromide ($[\text{NBu}_4]\text{Br}$), tetrabutylammonium iodide ($[\text{NBu}_4]\text{I}$), phenanthrene, propiophenone, 4-chlorotoluene and sodium tertbutoxide were purchased from Aldrich. Bis(triphenylphosphine)iminium chloride ($[\text{PPN}]\text{Cl}$) and 1,1'-bis(di-*tert*-butylphosphino)ferrocene (dtbpf) were purchased from Strem Chemicals, Inc. Sodium bromide, sodium iodide and THF-d8 were purchased from Fisher Scientific. Lithium tetrakis(pentafluorophenyl)borate etherate and potassium tetrakis(pentafluorophenyl)borate ($\text{K}[\text{TFAB}]$) were purchased from Boulder Scientific. Tetrabutylammonium hexafluorophosphate ($[\text{NBu}_4][\text{PF}_6]$) was purchased from Aldrich and dried under vacuum at 100°C prior to use. Ferrocene (FcH) was purchased from Strem and sublimed prior to use. The compounds sodium tetrakis(3,5-bis(trifluoromethyl)phenyl)borate ($\text{Na}[\text{BArF}]$),³⁸ $[\text{Pd}(\text{dtbpf})\text{Cl}_2]$,³⁹ tetrabutylammonium tetrakis(pentafluorophenyl)borate ($[\text{NBu}_4][\text{TFAB}]$),⁴⁰ and $[\text{Pd}(\text{dtbpf})\text{I}][\text{I}]$ ¹⁸ were prepared according to literature procedures. All reactions were carried out under argon using standard Schlenk techniques unless otherwise noted. Methylene chloride (CH_2Cl_2), hexanes and diethyl ether (Et_2O) were purified using a Solv-Tek purification system similar to the one previously described.⁴¹ Acetone and benzene were degassed and purged with argon prior to use. THF was distilled from potassium benzophenone ketyl under argon prior to use. A JEOL Eclipse 400 FT-NMR spectrometer was used to acquire the $^{31}\text{P}\{^1\text{H}\}$ NMR and ^1H NMR spectra. The ^1H NMR spectra were referenced to TMS ($\delta = 0.00$ ppm). Chemical shifts of the $^{31}\text{P}\{^1\text{H}\}$ NMR spectra are referenced to an external sample of 85% H_3PO_4 . GC-MS data were obtained using a VG/FISONS Model MD800 gas chromatograph/mass spectrometer. All reported yields are isolated yields. Elemental analysis was performed by Quantitative Technologies, Inc.

Synthesis of [Pd(dtbpf)Cl][TFAB]. K[TFAB] (0.0891 g, 0.124 mmol) was added to a brown-orange solution of [Pd(dtpbf)Cl₂] (0.0778 g, 0.119 mmol) in 10 mL of CH₂Cl₂. The reaction changed color to a darker brown-orange while stirring for 15 minutes. The solution was then filtered and solvent was removed from the filtrate *in vacuo*. The residue was triturated with ether (3 x 5 mL) and dried under vacuum. The product was obtained as a black solid (0.0943 g, 61% yield). ¹H NMR (CDCl₃): δ (ppm) 5.19 (br s, 4H, H_β), 3.96 (br s, 4H, H_α), 1.53 (br s, 36H, -CH₃). ³¹P{¹H} NMR (CDCl₃) δ 9.8 (s). Anal. Calcd for C₅₀H₄₄BClF₂₀Fe₁P₂Pd₁: C, 46.36; H, 3.42. Found: C, 46.12, H, 3.21.

Reaction of [Pd(dtbpf)Cl][TFAB] with [PPN]Cl. In an NMR tube reaction, [Pd(dtbpf)Cl][TFAB] (0.0089 g, 6.9 μmol) and [PPN]Cl (0.0040 g, 7.0 μmol) were dissolved in CH₂Cl₂ (1 mL). This resulted in a brown solution. ³¹P{¹H} NMR (CH₂Cl₂): δ 67.7 (s), 21.6 (s).

Reaction of [Pd(dtbpf)Cl][TFAB] with [NBu₄]Br. [Pd(dtbpf)Cl][TFAB] (0.0280 g, 22.6 μmol) and [NBu₄]Br (0.0073 g, 23 μmol) were placed in an NMR tube and dissolved in CH₂Cl₂ (1 mL). ³¹P{¹H} NMR (CH₂Cl₂): δ 67.7 (s), 15.1 (s).

Reaction of [Pd(dtbpf)Cl][TFAB] with [NBu₄]I. [Pd(dtbpf)Cl][TFAB] (0.0221 g, 17.8 μmol) and [NBu₄]I (0.0066 g, 18 μmol) were placed in an NMR tube and dissolved in CH₂Cl₂ (1 mL). ³¹P{¹H} NMR (CH₂Cl₂): δ 67.7 (s), 10.9 (s).

Synthesis of [Pd(dtbpf)Br][TFAB]. [NBu₄]Br (0.0095 g, 30 μmol) was dissolved in 5 mL methylene chloride. In a separate flask [Pd(dtbpf)Cl][TFAB] (0.0382 g, 29.5 μmol) was dissolved in 10 mL methylene chloride. The [Pd(dtbpf)Cl][TFAB] solution was slowly added over 10 minutes to the [NBu₄]Br solution and the resulting solution was stirred 10 min. The solution was then layered with 20 mL hexanes and placed in the freezer overnight. This yielded a black precipitate and an orange solution. The solution was filtered and the solid was washed with

5 mL of ether and the dried *in vacuo*. The product was collected as a black solid (0.0170 g, 43% yield) ^1H NMR (CDCl_3): δ (ppm) 6.32 (br s, 4H, H_β), 4.15 (br s, 4H, H_α), 1.54 (br s, 36H, $-\text{CH}_3$). $^{31}\text{P}\{^1\text{H}\}$ NMR (CDCl_3) δ 11.5 (s). Anal. Calcd for $\text{C}_{50}\text{H}_{44}\text{BBrF}_{20}\text{Fe}_1\text{P}_2\text{Pd}_1$: C, 44.82; H, 3.31. Found: C, 44.90, H, 3.30.

Synthesis and Characterization of $[\text{Pd}(\text{dtbpf})\text{Br}][\text{Br}]$. $[\text{Pd}(\text{dtbpf})\text{Cl}_2]$ (0.3798 g, 0.583 mmol) and sodium bromide (0.3025 g, mmol) were placed in a flask and degassed. Acetone (15 mL) was added giving a dark grayish-red solution that was stirred for 22 h. The solvent was removed *in vacuo* and the resulting residue was triturated with 2 x 5 mL of DI water. The resulting product was azeotropically dried with benzene (50 mL) which was then removed *in vacuo*. The remaining solid was dissolved in minimal CH_2Cl_2 and layered with hexanes. The resulting solution was placed in the freezer overnight yielding a dark red-black precipitate. The solution was filtered, washed with 2 x 5 mL of Et_2O and dried *in vacuo* which yielded 0.2591 g (59%) of the product as a black solid. ^1H NMR (CDCl_3): δ (ppm) 6.32 (br s, 4H, H_β), 4.15 (br s, 4H, H_α), 1.54 (br s, 36H, $-\text{CH}_3$). $^{31}\text{P}\{^1\text{H}\}$ NMR (CDCl_3) δ 11.5 (s). Anal. Calcd for $\text{C}_{26}\text{H}_{44}\text{Br}_2\text{Fe}_1\text{P}_2\text{Pd}_1$: C, 42.16; H, 5.99. Found: C, 42.22, H, 6.09.

X-ray Diffraction Studies. Crystals of $[\text{Pd}(\text{dtbpf})\text{Br}][\text{TFAB}]$ were obtained at room temperature by vapor diffusion of Et_2O into a solution of each compound in CH_2Cl_2 . A Bruker-AXS Kappa APEX II CCD diffractometer with 0.71073 Å Mo- K_α radiation was used for collecting X-ray diffraction data. A single red-orange crystal (0.33 x 0.19 x 0.11 mm³) were selected and mounted using super glue onto a glass fiber and cooled to 100 K with a stream of dry nitrogen gas. A second sample was used to record data at a variety of temperatures (Supporting Information). Cell parameters were retrieved using APEX II software⁴² and refined using SAINT⁴³ on all observed reflections. Unit cell parameters were obtained from 60 data

frames, $0.5^\circ \Phi$, from three different sections of the Ewald sphere. The data set was treated with SADABS⁴⁴ absorption corrections based on redundant multi-scan data. The structure was solved by direct methods and refined by least squares method on F^2 using the SHELXTL program package.⁴⁵ All hydrogen atoms were treated as idealized contributions. Excepted as noted, all non-hydrogen atoms were refined with anisotropic displacement parameters. The systematic absences were consistent with the centrosymmetric, monoclinic space group $P2_1/n$. The data set consisted of 69951 reflections (13516 unique, $R_{int} = 0.0896$) collected over $\theta = 1.746$ to 28.282° . The monoclinic crystal has an asymmetric unit that contains one molecule of the $[\text{Pd}(\text{dtbpf})\text{Br}]^+$ cation and one $[\text{TFAB}]^-$ anion. After completing an anisotropic model of the molecule, there remained large residual electron density peaks around the palladium, iron, and bromine atoms that suggested a second isomer was present as a minor component. Alternate sites for the Pd, Fe, Br, and P centers were located in the Fourier difference maps and were modeled as isotropic atoms whose relative occupancy was refined to keep unit cell contents constant. The minor component occupancy of the heavy atoms refined to 9%. The light atoms of the minor component were not modeled and the occupancies of the corresponding major component were fixed at 1.0. This two isomer model gave a goodness of fit on F^2 of 1.032 with $R_1 = 4.28\%$ [$I > 2\sigma(I)$], $wR_2 = 9.76\%$ (all data) and with a largest difference peak and hole of 0.746 and -0.887 $e/\text{\AA}^3$. Reported measurements were taken using OLEX2.⁴⁶

Zero-field ^{57}Fe Mössbauer spectroscopy. Spectra were collected at various temperatures by restraining the desired sample in Paratone-N oil. The data were measured with a constant acceleration spectrometer (SEE Co., Minneapolis, MN). Isomer shifts are given relative to α -Fe metal at 298 K. Data were analyzed using an in-house package written by Evan R. King in Igor Pro (Wavemetrics). γ refers to the full-width-at-half-maximum.

Electrochemical Procedure. Cyclic voltammetry was performed using a CH Instruments Model CHI260D potentiostat at room temperature (21 ± 1 °C). Scans for [Pd(dtbpf)Br][Br] were conducted under an argon atmosphere. The analyte was 1.0 mM in CH₂Cl₂ (10.0 mL) and the supporting electrolyte was 0.1 M [NBu₄][PF₆]. Scans for [Pd(dtbpf)Cl][TFAB] were performed in an argon filled glove box. The analyte was 1.0 mM in CH₂Cl₂ (10.0 mL) and the supporting electrolyte was 0.05 M [NBu₄][TFAB]. All experiments were performed with glassy carbon working electrode (1.0 mm disk) that was polished with 1.0 μm then 0.25 μm diamond paste and rinsed with CH₂Cl₂ prior to use. The experiments also employed a non-aqueous Ag/AgCl pseudo-reference electrode which was separated from the solution by a frit and a platinum wire counter electrode. FcH was added at the end of the experiments and used as an internal reference. Data were background subtracted. Experiments were conducted at scan rates of 50 mV/s and 100 – 1000 mV/s in 100 mV/s increments. All data are reported at a scan rate of 100 mV/s.

Computational Studies. All structures were optimized using the ADF2013.01 software suite.⁴⁷ Full molecules were used for calculations. Optimizations were performed PW91⁴⁸ theory level, with full electron (no frozen cores) triple- ζ -potential (TZP) basis sets and using the relativistic scalar ZORA approximation. Mayer bond orders and atomic properties were calculated using the defaults implemented in the ADF2013.01 program suite. The optimized coordinates were used for further analysis with NBO 6.0 and Bader's Atoms In Molecules (AIM) methods, implemented in ADF.

Catalytic Studies. The reactions were performed under argon in THF (1.5 mL) with 1.5 mmol of 4-chlorotoluene, 1.65 mmol of propiophenone, 1.65 mmol of sodium tertbutoxide and 0.03 mmol of the desired palladium complex. The reactions were stirred and heated for 3 h at 60 °C before being allowed to cool to room temperature. A 100 μL sample of the reaction mixture

was diluted in 1.00 mL of a THF solution of phenanthrene (~ 7 mg). The sample was then injected into a CG-MS and the concentration of the desired product was determined. Reactions were performed three independent times with each catalyst.

ASSOCIATED CONTENT

Supporting Information

Tables, figures, CIF files giving crystallographic data, computational results and whatever else ends up there. This material is available free of charge via the Internet at <http://pubs.acs.org>.

AUTHOR INFORMATION

Corresponding Author

*E-mail: nataroc@lafayette.edu

Additional Author Information

Notes

The authors declare no competing financial interest.

ACKNOWLEDGEMENTS

This work was supported by the National Science Foundation (CHE-1057795). We thank the Kresge Foundation for the purchase of the JOEL NMR and the Academic Research Committee at Lafayette College for support through the EXCEL scholars program. R.H.S Acknowledges Consejo Nacional de Ciencia y Tecnología (CONACYT) and Fundación México for a doctoral fellowship.

References

- (1) (a) Gan, K.-S.; Hor, T. S. A. 1,1'-Bis(diphenylphosphino)ferrocene - Coordination Chemistry, Organic Synthesis and Catalysis. In *Ferrocenes: Homogeneous Catalysis, Organic Synthesis, Materials Science*; Togni, A., Hayashi, T., Eds.; VCH: Weinheim, Germany, 1995; pp 3-104. (b) Hayashi, T. Asymmetric Catalysis with Chiral Ferrocenylphosphine Ligands. In *Ferrocenes: Homogeneous Catalysis, Organic Synthesis, Materials Science*; Togni, A., Hayashi, T., Eds.; VCH: Weinheim, Germany, 1995; pp 105-142. (c) Chien, S. W.; Hor, T. S. A. The Coordination and Homogeneous Catalytic Chemistry of 1,1'-Bis(diphenylphosphino)ferrocene and its Chalcogenide Derivatives. In *Ferrocenes: Ligands, Materials and Biomolecules*; Štěpnička, P., Ed.; John Wiley & Sons Ltd.: West Sussex, England, 2008; pp 33-116. (d) Colacot, T. J.; Parisel, S. Synthesis, Coordination Chemistry and Catalytic Use of dppf Analogs. In *Ferrocenes: Ligands, Materials and Biomolecules*; Štěpnička, P., Ed.; John Wiley & Sons Ltd.: West Sussex, England, 2008; pp 117-140. (e) Štěpnička, P. 1'-Functionalized Ferrocene Phosphines: Synthesis, Coordination Chemistry and Catalytic Applications. In *Ferrocenes: Ligands, Materials and Biomolecules*; Štěpnička, P., Ed.; John Wiley & Sons Ltd.: West Sussex, England, 2008; pp 177-204. (f) Blaser, H.-U.; Chen, W.; Camponovo, F.; Togni, A. Chiral 1,2-Disubstituted Ferrocene Diphosphines for Asymmetric Catalysis. In *Ferrocenes: Ligands, Materials and Biomolecules*; Štěpnička, P., Ed.; John Wiley & Sons Ltd.: West Sussex, England, 2008; pp 205-236.
- (2) (a) Nataro, C.; Campbell, A. N.; Ferguson, M. A.; Incarvito, C. D.; Rheingold, A. L. *J. Organomet. Chem.* **2003**, *673*, 47. (b) Ong, J. H. L.; Nataro, C.; Golen, J. A.; Rheingold, A. L. *Organometallics* **2003**, *22*, 5027. (c) Hagopian, L. E.; Campbell, A. N.; Golen, J. A.; Rheingold, A. L.; Nataro, C. *J. Organomet. Chem.* **2006**, *691*, 4890. (d) Blanco, F. N.; Hagopian, L. E.; McNamara, W. R.; Golen, J. A.; Rheingold, A. L.; Nataro, C. *Organometallics* **2006**, *25*, 4292.
- (3) (a) Clavier, H.; Nolan, S. P. *Chem. Commun.* **2010**, *46*, 841. (b) Fey, N.; Harvey, J. N.; Lloyd-Jones, G. C.; Murray, P.; Orpen, A. G.; Osborne, R.; Purdie, M. *Organometallics* **2008**, *27*, 1372. (c) Landis, C. R.; Nelson, R. C.; Jin, W.; Bowman, A. C. *Organometallics* **2006**, *25*, 1377.
- (4) Damian, K.; Clarke, M. L.; Cogley, C. J. *App. Organomet. Chem.* **2009**, *23*, 272.
- (5) Milton, E. J.; Clarke, M. L. *Green Chem.* **2010**, *12*, 381.
- (6) Wang, Y.; Liu, L.; Wang, D.; Chen, Y.-J. *Org. Biomol. Chem.* **2012**, *10*, 6908.
- (7) Ashfield, L.; Barnard, C. F. J. *Org. Process Res. Dev.* **2007**, *11*, 39.
- (8) Slatford, P. A.; Whittlesey, M. K.; Williams, J. M. J. *Tet. Lett.* **2006**, *47*, 6787.
- (9) Swartz, B. D.; Nataro, C. *Organometallics* **2005**, *24*, 2447.
- (10) Mann, G.; Shelby, Q.; Roy, A. H.; Hartwig, J. F. *Organometallics* **2003**, *22*, 2775.
- (11) Kawatsura, M.; Hartwig, J. F. *J. Am. Chem. Soc.* **1999**, *121*, 1473.
- (12) Ramos, A.; Lough, A. J.; Stephan, D. W. *Chem. Commun.* **2009**, 1118.
- (13) Zuideveld, M.A.; Swennenhuis, B.H.G.; Kamer, P.C.J.; van Leeuwen, P.W.N.M. *J. Organomet. Chem.* **2001**, *637*, 805.
- (14) Gramigna, K. M.; Oria, J. V.; Mandell, C. M.; Tiedemann, M. A.; Dougherty, W. G.; Piro, N. A.; Kassel, W. S.; Chan, B. C.; Diaconescu, P. L.; Nataro, C. *Organometallics* **2013**, *32*, 5966.
- (15) Colacot, T. J.; Shea, H. A. *Org. Lett.* **2004**, *6*, 3731.

- (16) Bennett, M. A.; Bhargava, S. K.; Bond, A. M.; Bansal, V.; Forsyth, C. M.; Guo, S.-X.; Privér, S. H. *Inorg. Chem.* **2009**, *48*, 2593.
- (17) (a) Grasa, G. A.; Colacot, T. J. *Org. Lett.* **2007**, *9*, 5489. (b) Grasa, G. A.; Colacot, T. J. *Org. Process Res. Dev.* **2008**, *12*, 522.
- (18) Fillion, E.; Taylor, N. J. *J. Am. Chem. Soc.* **2003**, *125*, 12700.
- (19) Cordero, B.; Gomez, V.; Platero-Prats, A. E.; Reves, M.; Echeverria, J.; Cremades, E.; Barragan, F.; Alvarez, S. *Dalton Trans.* **2008**, 2832.
- (20) (a) Poater, A.; Cosenza, B.; Correa, A.; Giudice, S.; Ragone, F.; Scarano, V.; Cavallo, L. *Eur. J. Inorg. Chem.* **2009**, 1759. (b) <http://www.molnac.unisa.it/OMtools/sambvca.php>.
- (21) Sohn, Y. S.; Hendrickson, D. N.; Gray, H. B. *J. Am. Chem. Soc.* **1971**, *93*, 3603.
- (22) Sato, M.; Shigeta, H.; Sekino, M.; Akabori, S. *J. Organomet. Chem.* **1993**, *458*, 199.
- (23) Sato, M.; Sekino, M.; Katada, M.; Akabori, S. *J. Organomet. Chem.* **1989**, *377*, 327.
- (24) Green, A. G.; Kiesz, M. D.; Oria, J. V.; Elliott, A. G.; Buechler, A. K.; Hohenberger, J.; Meyer, K.; Zink, J. I.; Diaconescu, P. L. *Inorg. Chem.* **2013**, *52*, 5603.
- (25) Zuideveld, M. A.; Swennenhuis, B. H. G.; Boele, M. D. K.; Guari, Y.; van Strijdonck, G. P. F.; Reek, J. N. H.; Kamer, P. C. J.; Goubitz, K.; Fraanje, J.; Lutz, M.; Spek, A. L.; van Leeuwen, P. W. N. M. *Dalton Trans* **2002**, 2308.
- (26) Houlton, A.; Bishop, P. T.; Roberts, R. M. G.; Silver, J.; Herberhold, M. *J. Organomet. Chem.* **1989**, *364*, 381.
- (27) Bickar, D.; Lukas, B.; Neshvad, G.; Roberts, R. M. G.; Silver, J. *J. Organomet. Chem.* **1984**, *263*, 225.
- (28) Houlton, A.; Ibrahim, S. K.; Dilworth, J. D.; Silver, J. *J. Chem. Soc. Dalton Trans.*, **1990**, 2421.
- (29) Appleton, T. D.; Cullen, W. R.; Evans, S. V.; Kim, T.-J.; Trotter, J. *J. Organomet. Chem.* **1985**, *279*, 5.
- (30) (a) Seyferth, D.; Hames, B. W.; Rucker, T. G.; Cowie, M.; Dickson, R. S. *Organometallics* **1983**, *2*, 472. (b) Cowie, M.; Dickson, R. S. *J. Organomet. Chem.* **1987**, *326*, 269.
- (31) Sato, M.; Asano, H.; Suzuki, K.; Katada, M.; Akabori, S. *Bull. Chem. Soc. Jpn.* **1989**, *62*, 3828.
- (32) Sato, M.; Suzuki, K.; Asano, H.; Sekino, M.; Kawata, Y.; Habata, Y.; Akabori, S. *J. Organomet. Chem.* **1994**, *470*, 263.
- (33) McCulloch, B.; Ward, D. L.; Woolins, J. D.; Brubaker, C. H. *Organometallics* **1985**, *4*, 1425.
- (34) (a) Reinisch, L.; Heidemeier, J.; Parak, F. *Eur. Biophys. J.* **1985**, *12*, 167. (b) Grandjean, F.; Long, G. J.; Benson, C. G.; Russo, U. *Inorg. Chem.* **1988**, *27*, 1524.
- (35) Silver, J. *Dalton Trans.* **1990**, 3513.
- (36) Roberts, R. M. G.; Silver, J. *J. Organomet. Chem.* **1984**, *263*, 235.
- (37) Both papers in reference 17 state that the catalysts were purchased from Johnson Matthey, Catalysis and Chiral Technologies. The company website lists both dibromo[1,1'-bis(di-tert-butylphosphino)ferrocene]palladium(II) and diiodo[1,1'-bis(di-tert-butylphosphino)ferrocene]palladium(II), but only the structure of the iodide is shown and it is correctly presented as [Pd(dtbpf)I][I]. (http://jmctt.com/products-services/product_p161.html accessed August 13, 2015).
- (38) Yakelis, N. A.; Bergman, R. G. *Organometallics*, **2005**, *24*, 3579.
- (39) Butler, I. R.; Cullen, W. R.; Kim, T.-J.; Rettig, S. J.; Trotter, J. *Organometallics* **1985**, *4*, 972.

- (40) LeSuer, R.; Geiger, W. E. *Angew. Chem. Int. Ed. Engl.* **2000**, *39*, 248.
- (41) Pangborn, A. B.; Giardello, M. A.; Grubbs, R. H.; Rosen, R. K.; Timmers, F. J. *Organometallics* **1996**, *15*, 1518.
- (42) APEX II, v. 2012.10-0; Bruker AXS: Madison, WI, 2012.
- (43) SAINT+, v. 8.26A: Data Reduction and Correction Program; Bruker AXS: Madison, WI, 2011.
- (44) SADABS, v. 2012/1: An Empirical Absorption Correction Program; Bruker AXS Inc.: Madison, WI, 2012.
- (45) Sheldrick, G. M. SHELXTL, v. 2012.10-2: Structure Determination Software Suite; Bruker AXS Inc.: Madison, WI, 2012.
- (46) Dolomanov, O. V.; Bourhis, L. J.; Gildea, R. J.; Howard, J. A. K.; Puschmann, H. *J. Appl. Cryst.* **2009**, *42*, 339.
- (47) (a) ADF2013.01; SCM; <http://www.scm.com>: Theoretical Chemistry, Vrije Universiteit, Amsterdam, The Netherlands. (b) te Velde, G.; Bickelhaupt, F. M.; Baerends, E. J.; Fonseca Guerra, C.; van Gisbergen, S. J. A.; Snijders, J. G.; Ziegler, T. *J. Comput. Chem.* **2001**, *22*, 931. (c) Fonseca Guerra, C.; Snijders, J. G.; te Velde, G.; Baerends, E. *J. Theor. Chem. Acc.* **1998**, *99*, 391.
- (48) Perdew, J. P.; Wang, Y. *Phys. Rev. B* **1992**, *45*, 13244.
- (49) (a) Mayer, I. *Chem. Phys. Lett.* **1983**, *97*, 270. (b) Bridgeman, A. J.; Cavigliasso, G.; Ireland, L. R.; Rothery, J. *J. Chem. Soc., Dalton Trans.* **2001**, 2095.
- (50) Niskanen, M.; Hirva, P.; Haukka, M. *J. Chem. Theory Comput.* **2009**, *5*, 1084.
- (51) Glendening, E. D.; Badenhoop, J. K.; Reed, A. E.; Carpenter, J. E.; Bohmann, J. A.; Morales, C. M.; Landis, C. R.; Weinhold, F. <http://nbo6.chem.wisc.edu>: Theoretical Chemistry Institute, University of Wisconsin, Madison, WI, 2013.
- (52) (a) Bader, R. F. W. *Atoms in Molecules - A Quantum Theory*; Oxford University Press: Oxford, 1990. (b) Rodríguez, J. I.; Bader, R. F. W.; Ayers, P. W.; Michel, C.; Götz, A. W.; Bo, C. *Chem. Phys. Lett.* **2009**, *472*, 149.
- (53) Fowe, E. P.; Therrien, B.; Suss-Fink, G.; Daul, C. *Inorg. Chem.* **2007**, *47*, 42.
- (54) Makal, A. M.; Plazuk, D.; Zakrzewski, J.; Misterkiewicz, B.; Wozniak, K. *Inorg. Chem.* **2010**, *49*, 4046.

For Table of Contents Use only

A variety of compounds possessing an interaction between the metal center of a 1,1'-bis(phosphino)metallocene ligand and a group 10 metal center have been prepared. The nature of the metal-metal interaction is examined using crystallographic, spectroscopic, computational and electrochemical methods.